RSC Advances

COMMUNICATION

View Article Online
View Journal | View Issue

Cite this: *RSC Adv.*, 2016, **6**, 54539

Received 22nd April 2016
Accepted 28th May 2016

DOI: 10.1039/c6ra10430d

www.rsc.org/advances

Hierarchical hybrid nanostructures: controlled assembly of polymer-encapsulated gold nanoparticles *via* a Rayleigh-instability-driven transformation under cylindrical confinement†

Hao-Wen Ko, Chun-Wei Chang, Mu-Huan Chi, Chien-Wei Chu, Ming-Hsiang Cheng, Zhi-Xuan Fang, Ke-Hsuan Luo and Jiun-Tai Chen*

We develop a novel route based on the solution wetting method using anodic aluminum oxide (AAO) templates to fabricate hierarchical hybrid nanostructures assembled from polystyrene-encapsulated gold nanoparticles (Au@PS NPs). Hybrid nanostructures including nanotubes and nanospheres can be reliably prepared, in which the spatial arrangement of the Au@PS NPs is determined by the pore diameters of the templates and the molecular weights of the thiol-ended polystyrene (PS-SH) ligands. In particular, the Rayleigh-instability-driven transformation plays a key role in the formation of the hybrid nanospheres.

In recent years, there has been growing interest in assembling functional nanoparticles (NPs) into hierarchical hybrid nanomaterials, which usually possess unusual properties and can be applied to a wide range of applications, such as sensing, drug delivery, photocatalysis, and organic solar cells.[1–5] Several methods have been developed to encapsulate functional nanoparticles into inorganic materials or polymers.[6,7] Moreover, hierarchical hybrid nanomaterials can be used as building blocks for molecular assembly through molecular recognition, templates, chemical binding, or external forces.[8–10] Although considerable progress has been achieved to fabricate hybrid nanomaterials containing functional NPs, it is still a great challenge to precisely control not only the morphologies of the nanomaterials but also the spatial arrangement of the functional NPs.

In this work, we develop a novel solution template wetting method to fabricate hierarchical hybrid nanostructures containing polymer-encapsulated gold NPs (AuNPs). Previously, the preparation of AuNP clusters has been reported using different methods.[11,12] Here, polystyrene-encapsulated AuNPs (Au@PS NPs) are first prepared by directly conjugating the thiol-ended polystyrene (PS-SH) to the surfaces of AuNPs *via* strong thiol–gold bonding and used as building blocks for the directed-assembly process. The solutions containing the Au@PS NPs are infiltrated into the nanopores of anodic aluminum oxide (AAO) templates, and hybrid nanotubes can be formed after the evaporation of the solvents. Moreover, hierarchical hybrid nanospheres can be prepared by a Rayleigh-instability-driven transformation using a nonsolvent infiltrating process. The morphologies of the hybrid nanostructures are characterized by electron microscopy, and the optical properties related to the localized surface plasmon resonance (LSPR) are also investigated.

The strategy used in this work for preparing hybrid nanostructures is an advanced version of the conventional template wetting method, a powerful approach for making one-dimensional nanomaterials.[13,14] Compared to other templates, the AAO membrane is one of the most widely used templates because of the well-ordered nanopores with tunable pore diameters, pore-to-pore distances, and pore lengths.[15,16] Using the AAO templates, nanostructures with unique morphologies and properties, which are imposed by the cylindrical confinement of the nanopores and are not commonly observed in the bulk state, have been fabricated.[17,18] For making polymer nanostructures using templates, there are generally four major wetting-based methods to introduce polymers into the nanopores, including the melt wetting method, the solution wetting method, the solvent vapor annealing wetting method, and the microwave annealing wetting method.[19–23] Polymer nanomaterials can be fabricated and released after the polymers are solidified in the nanopores and the AAO templates are selectively removed. Among these methods, the solution wetting method is considered as the most versatile method because it provides more experimental parameters for controlling the morphologies and properties of polymer nanomaterials, such as the concentration of solution, the type of solvent, the immersing time, the interfacial tension, and the drying condition.[20,24–26] For example, polymer nanostructures with distinct morphologies such as peapod-like or candied-gourd-like

Department of Applied Chemistry, National Chiao Tung University, Hsinchu, Taiwan 30010. E-mail: jtchen@mail.nctu.edu.tw; Tel: +886-3-5731631

† Electronic supplementary information (ESI) available: Experimental section, images of AuNPs and AAO templates, and UV-vis spectra of AuNP solutions. See DOI: 10.1039/c6ra10430d

nanostructures can be prepared by controlling the solvent and the immersing times using the solution wetting method.[27,28]

There are four main advantages of using the solution template wetting method to prepare hierarchical hybrid Au@PS nanostructures. First, the sizes of the hybrid Au@PS nanostructures can be tuned by adjusting the pore diameters of the AAO templates. Second, the optical properties of the hybrid nanostructures can be controlled by changing the interparticle distances using PS-SH ligands with different molecular weights. Third, the number of AuNPs contained in a hybrid Au@PS nanostructures can be controlled by using AAO templates with different pore diameters and using ligands with different molecular weights. Fourth, it may be possible to cover a hybrid nanostructures with other polymers for the fabrication of hybrid core–shell nanostructures. This work not only provides a novel concept to prepare hierarchical hybrid nanostructures combining functional NPs and polymers with controlled morphologies, but also gives a deeper understanding on the relations between the morphologies and optical properties of nanomaterials.

Fig. 1 shows the graphical illustration for the assembly of polymer-encapsulated AuNPs and the experimental processes to prepare the hierarchical hybrid nanostructures by the assembly of polymer-encapsulated AuNPs. AuNPs are selected in this work because of their fundamental and applied aspects relevant to the quantum size effect.[29] For example, the surface plasmon resonance of AuNPs is strongly dependent on the shape of the nanoparticles, the particle size, the interparticle distance, and the nature of the protecting organic shell. Another practical reason for selecting Au is the electron density difference between AuNPs and polymers, enabling easier observation of the hybrid nanostructures using TEM measurement. Moreover, the optical properties related to the LSPR of AuNPs can be observed by UV-vis measurement. Au@PS NPs are used as building blocks to form hierarchical hybrid Au@PS nanotubes and nanospheres (Fig. 1a). AuNPs of a uniform size with citrate ligands are prepared by a citrate reduction method.[30,31] After the ligand-exchange process, the ligands on the surfaces of AuNPs are exchanged by PS-SH to form Au@PS NPs.[32,33]

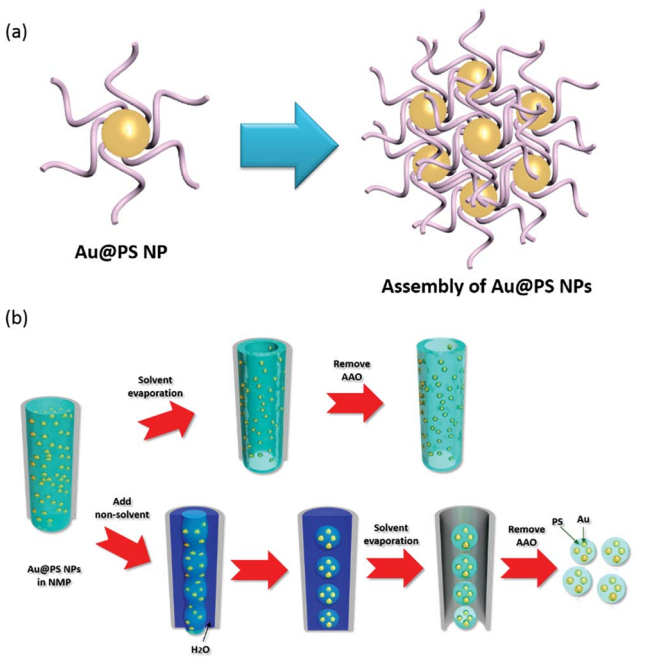

Fig. 1 (a) Graphical illustration for the assembly of polymer-encapsulated AuNPs. (b) Graphical illustration of the experimental processes to prepare hierarchical hybrid nanostructures by the assembly of polymer-encapsulated AuNPs.

For preparing hybrid nanotubes, the nanopores of AAO templates are wetted by Au@PS NP solutions *via* the solution wetting method. Because of the high surface energy of AAO templates, the Au@PS NP solutions can easily wet the nanopores through the capillary force. After the solvents are evaporated completely, the Au@PS NPs are deposited on the AAO walls. By removing the AAO templates selectively using 5 wt% NaOH(aq), hybrid nanotubes can be obtained, as illustrated in the upper part of Fig. 1b.

For making hierarchical hybrid Au@PS nanospheres, a unique nonsolvent-induced morphology transformation is applied. After the nanopores of AAO templates are wetted by Au@PS NP solutions, water (acting as a nonsolvent) is introduced into the nanopores. Because of the stronger interaction between water and the surfaces of AAO nanopores than that between Au@PS NP solutions and the surfaces of AAO nanopores, the Au@PS NP solutions are isolated in the center of the AAO nanopores. The isolated solution cylinders then transform into spherical solution domains, induced by the Rayleigh-instability-driven transformation process, which reduce the surface energies between the solution and water.[34–37] After the solvents are dried and the AAO templates are removed selectively by NaOH(aq), hierarchical hybrid nanospheres containing Au@PS NPs can be obtained, as illustrated in the lower part of Fig. 1b. The morphologies of the hybrid nanostructures are characterized by scanning electron microscopy (SEM) and transmission electron microscopy (TEM). Their optical properties are examined by ultraviolet-visible (UV-vis) spectroscopy, which can be used to investigate the effect of LSPR of the nanostructures.

For typical experiments, AuNPs protected by sodium citrates and monodispersed in water are first prepared using a citrate reduction process, as reported previously.[30,31] The TEM images of the citrate-capped AuNPs (Au@citrate) are shown in Fig. S1,† where the average size is ~11.4 nm. The citrates on the surfaces of the AuNPs are then replaced by PS-SH *via* a ligand exchange process to fabricate Au@PS NPs (details of the experimental process are described in the ESI†).[32,33]

Fig. S2† shows the TEM images of Au@PS NPs monolayers prepared by casting Au@PS NP solutions in toluene on copper grids, followed by a solvent evaporation process.[38] For PS-SH with different molecular weights, the thicknesses of the PS shells can be tuned. Here, we use PS-SH with molecular weights of 5.8 and 53 kg mol^{-1} to prepare the NPs (Au@$PS_{5.8k}$ and Au@PS_{53k}). The synthesized Au@PS NPs are expected to compose of AuNP cores and PS shells. Therefore, the sizes of the Au@PS NPs and the thicknesses of the PS shells can be estimated by measuring the average core-to-core distance of Au@PS

NPs monolayer from TEM images. Fig. S2a and b† show the monolayers of Au@$PS_{5.8k}$ NPs, where the average core-to-core distances between AuNPs is ~20.8 nm, indicating that the average thickness of the PS shells of the Au@$PS_{5.8k}$ NPs is ~4.7 nm. For the monolayers of AuNP with higher molecular weight PS-SH ligands (Au@PS_{53k} NPs), as shown in Fig. S2c and d,† the average core-to-core distance between AuNPs is increased to ~38.5 nm, indicating that the average thickness of the PS shells of the Au@PS_{53k} NPs is ~13.5 nm.

The optical properties of Au@citrate NP and Au@PS NP solutions are examined by UV-vis spectroscopy, as shown in Fig. S3.† The absorption peaks of the Au@citrate NP solution, Au@$PS_{5.8k}$ NP solution, and Au@PS_{53k} NP solution are 518, 531, and 529 nm, respectively. A significant red-shift of the absorption peak is observed for the PS-capped samples comparing to the citrate-capped samples. Briefly, AuNPs conjugated by PS-SH with different molecular weights not only have tunable interparticle distances in a solid state, but also have different optical properties in a solution state.

After characterizing the morphologies and optical properties of Au@PS NPs, we then apply the solution template wetting method to fabricate different hybrid nanostructures containing Au@PS NPs. AAO templates with two different average pore diameters (~60 and ~230 nm) are used in this work, as shown in Fig. S4.† By dipping the AAO templates into the Au@PS NP solutions followed by a solvent evaporation process, hybrid nanotubes containing Au@PS NPs can be successfully prepared. The infiltrating process of the Au@PS NP solution into the AAO nanopores is driven by the capillary force.[20] Because the AAO nanopores possess much higher surface energy than the Au@PS NP solutions do, the solutions spontaneously cover the surfaces of the AAO nanopores to lower the total surface energy; moreover, the small diameter of the AAO nanopores cause the Au@PS NP solutions to wet the nanopores within a few seconds. In the fabrication process, the residual solutions on the surfaces of the AAO templates are removed by a wiping step to avoid the formation of thick films outside the nanopores. This wiping process is critical because the formation of residual films can lead to misinterpretation on the morphologies and properties of the nanostructures.

The sizes of the hybrid nanotubes are controlled by the pore diameters of the AAO templates, as demonstrated in Fig. 2. When the pore diameters of the AAO templates decrease from 230 to 60 nm, the diameters of the hybrid nanotubes decrease correspondingly. For the nanotubes obtained by using AAO templates with the same pore diameters, the arrangements of the Au@PS NPs are affected by the AuNPs with different molecular weight PS-SH ligands (Au@$PS_{5.8k}$ NPs and Au@PS_{53k} NPs).

Then we apply the nonsolvent infiltrating process to further adjust the morphologies of the hybrid nanostructures from nanotubes to nanospheres.[36] In this process, the choice of the solvent and nonsolvent is critical and has several requirements. First, the solvent which dissolves the Au@PS NP should have a high boiling point and a slow evaporation rate to prevent fast solidification of the Au@PS NP solutions before the nonsolvent infiltrates the nanopores of the AAO templates. Second, the solvent and the nonsolvent should be miscible, so the nonsolvent

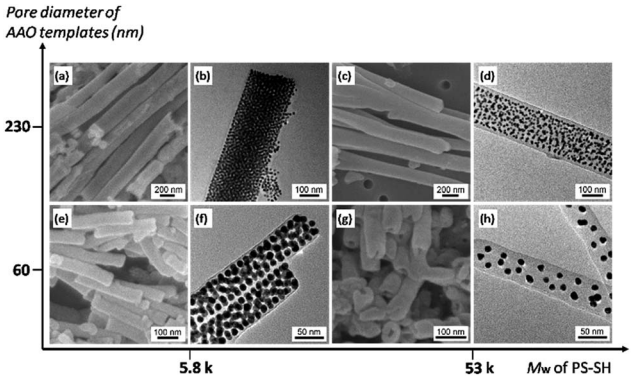

Fig. 2 SEM (a, c, e, and g) and TEM (b, d, f, and h) images of hybrid polymer nanotubes containing Au@PS NPs by adjusting the molecular weight of PS-SH and the pore diameter of AAO templates. (a and b) Hybrid polymer nanotubes containing Au@$PS_{5.8k}$ NPs with the pore diameter of 230 nm; (c and d) hybrid polymer nanotubes containing Au@PS_{53k} NPs with the pore diameter of 230 nm; (e and f) hybrid polymer nanotubes containing Au@$PS_{5.8k}$ NPs with the pore diameter of 60 nm; (g and h) hybrid polymer nanotubes containing Au@PS_{53k} NPs with the pore diameter of 60 nm.

can infiltrate the nanopores filled with Au@PS NP solutions. Third, the nonsolvent should have stronger interactions to the anodic aluminum oxide walls than the solvent does; therefore, the Au@PS NP solutions can be isolated in the center of the nanopores and undergo the subsequent Rayleigh-instability-driven transformation process to form the hierarchical hybrid nanospheres.

For fulfilling the above requirements, in this work, we choose *N*-methyl-2-pyrrolidone (NMP) and water as solvent (to dissolve Au@PS NPs) and nonsolvent (does not dissolve Au@PS NPs), respectively. After the Au@PS NP solutions infiltrate the nanopores of the AAO templates, the nonsolvent (water) is introduced into the nanopores before the Au@PS NP solutions are solidified. The stronger interactions between water and aluminum oxide walls than those between the Au@PS NP solutions and aluminum oxide walls cause the Au@PS NP solutions to be isolated in the center of the nanopores. The isolated cylindrical solution domains then transform to spherical solution domains *via* the Rayleigh-instability-driven transformation process. After the solvents evaporate, hierarchical hybrid Au@PS nanospheres can be prepared, as shown in Fig. 3. The diameters of the hierarchical hybrid nanospheres are mainly controlled by the pore sizes of the AAO templates while the distances between the AuNPs within a nanosphere is determined by the molecular weight of the PS-SH ligands that conjugated on the surfaces of AuNPs.

For calculating the number of AuNPs per hierarchical hybrid Au@PS nanosphere, we first assume that the average core-to-core distances between AuNPs in hierarchical hybrid Au@PS nanospheres are similar to those in Au@PS NP monolayers. In addition, the shapes of the Au@PS NP and the hierarchical hybrid Au@PS nanospheres are assumed to be spherical. The graphical illustrations of a Au@PS NP monolayer and a hierarchical hybrid Au@PS nanosphere are shown in Fig. S5.† The number of AuNPs per hierarchical hybrid Au@PS nanosphere

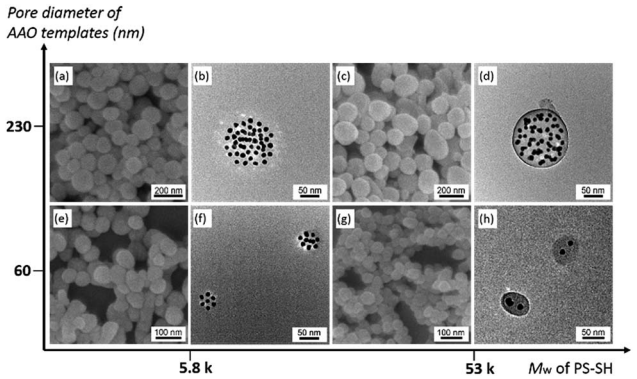

Fig. 3 SEM (a, c, e, and g) and TEM (b, d, f, and h) images of hierarchical hybrid Au@PS nanospheres by adjusting the molecular weight of PS-SH and the pore diameter of AAO templates. (a and b) Hierarchical hybrid nanospheres containing Au@$PS_{5.8k}$ NPs with the pore diameter of 230 nm; (c and d) hierarchical hybrid nanospheres containing Au@PS_{53k} NPs with the pore diameter of 230 nm; (e and f) hierarchical hybrid nanospheres containing Au@$PS_{5.8k}$ NPs with the pore diameter of 60 nm; (g and h) hierarchical hybrid nanospheres containing Au@PS_{53k} NPs with the pore diameter of 60 nm.

can therefore be estimated by measuring both the average sizes of the Au@PS NP and the hierarchical hybrid Au@PS nanospheres. The average sizes of the Au@$PS_{5.8k}$ NP, for example, can be obtained from the TEM images of Au@$PS_{5.8k}$ NP monolayers (Fig. S2a and b†). The average core-to-core distance of the nanoparticle is equal to the average diameter of the Au@$PS_{5.8k}$ NP (~20.8 nm); therefore, the average size of the Au@$PS_{5.8k}$ NP is ~37 675 nm^3. Similarly, the average sizes of the Au@PS_{53k} NP can be obtained from the TEM images of Au@PS_{53k} NP monolayers (Fig. S2c and d†). The average core-to-core distance of the nanoparticle is equal to the average diameter of the Au@PS_{53k} NP (~38.5 nm); therefore, the average size of the Au@PS_{53k} NP is ~238 919 nm^3.

For the average sizes of the hierarchical hybrid Au@PS nanospheres, they can be obtained by measuring the sizes of the nanospheres in the SEM images (Fig. 3a, c, e and g). Take hierarchical hybrid Au@PS_{53k} nanospheres prepared by using AAO templates with 60 nm pores for example, the average diameter is ~49.7 nm, corresponding to an average size of ~513 970 nm^3. By dividing the average size of hierarchical hybrid Au@PS_{53k} nanospheres (~513 970 nm^3) to the average size of Au@PS_{53k} NP (~238 919 nm^3), the average number of AuNPs inside a hierarchical hybrid Au@PS_{53k} nanospheres can be estimated to be ~2.2, which is in agreement with the TEM result (Fig. 3h). For hierarchical hybrid Au@PS nanospheres prepared by using AAO templates with different pore sizes (~60 nm and ~230 nm), the average numbers of AuNPs inside hierarchical hybrid Au@PS nanospheres can be estimated using similar procedures. The estimated numbers of the AuNPs in other cases of hierarchical hybrid Au@PS nanospheres also agree with the TEM results (Fig. 3b, d and f). The summarized results of the average numbers of AuNPs and sizes of hierarchical hybrid Au@PS nanospheres are shown in Table S1.†

Previously, Zhu and coworkers reported the assembly of Au@PS NPs under cylindrical confinement by immersing an AAO membrane in a solution of Au@PS NPs in chloroform, followed by evaporation of chloroform and solvent annealing under saturated chloroform atmosphere.[39] Interesting assemblies such as linear chain, zigzag, two-NP layer, three-NP layer, and hexagonally packed NP structures were observed; only cylinder-shape nanostructures were obtained. In contrast, here we use the solution wetting method and remove the residual Au@PS NP solution on the AAO template; the nanotubes containing Au@PS NPs can be obtained after the solvent evaporation process. Moreover, the solution wetting method is extended to the nonsolvent-induced morphology transformation to form nanospheres.

In addition to discuss the morphologies of the nanostructures and the arrangement of the Au@PS NPs, we further characterize the optical properties of these nanostructures. The UV-vis spectra of the Au@PS NP solutions in NMP and the hybrid nanostructures prepared by different conditions are shown in Fig. 4. For the samples with lower molecular weight ligands (Au@$PS_{5.8k}$), the absorption peaks of the nanostructure samples (Au@$PS_{5.8k}$-tube and Au@$PS_{5.8k}$-sphere, λ_{max} = 543 nm) are more red-shifted than that of the solution sample (Au@$PS_{5.8k}$-solution, λ_{max} = 531 nm), as shown in Fig. 4a. It has to be noted that the absorption peaks of the nanotube and the nanosphere samples are close because of the similar interparticle distances in both samples. Similar results are observed when the samples with higher molecular weight ligands (Au@PS_{53k}) are used.

For the samples with higher molecular weight ligands (Au@$PS_{5.8k}$), the absorption peaks of the nanostructure samples (Au@PS_{53k}-tube and Au@PS_{53k}-sphere, λ_{max} = 537 nm) are more red-shifted than that of the solution sample (Au@PS_{53k}-solution, λ_{max} = 529 nm), as shown in Fig. 4b. To see a clearer effect of the molecular weight of the ligands, the nanostructures samples with ligands of different molecular weights are plotted in Fig. 4c and d. For both the hybrid nanotube and hierarchical

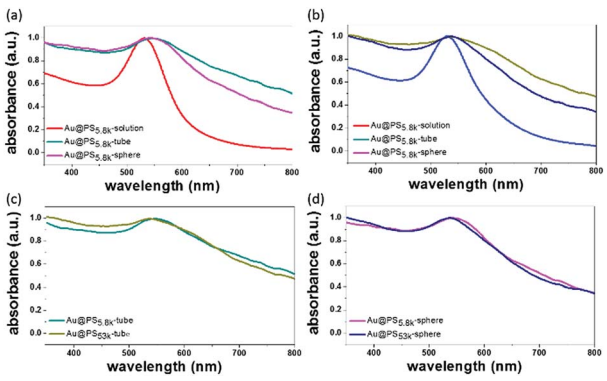

Fig. 4 UV-vis spectra of Au@PS NP solutions in NMP and nanostructures prepared by different conditions: (a) solutions and nanostructures containing Au@$PS_{5.8k}$ NPs, (b) solutions and nanostructures containing Au@PS_{53k} NPs, (c) hybrid polymer nanotubes containing Au@$PS_{5.8k}$ NPs and hybrid polymer nanotubes containing Au@PS_{53k} NPs, and (d) hierarchical hybrid nanospheres containing Au@$PS_{5.8k}$ NPs and hierarchical hybrid nanospheres containing Au@PS_{53k} NPs. The nanostructures containing Au@PS NPs are prepared using AAO templates with pore diameters of ~230 nm.

hybrid nanosphere samples, the absorption peaks, which characterized the frequency of LSPR, for the nanostructures with ligands of higher molecular weights are slightly blue-shifted than those for the nanostructures with ligands of lower molecular weights, which are due to the larger interparticle distances for the higher molecular weight samples. As the interparticle distances increase, the interactions of the interparticle dipole plasmon coupling become less effective, resulting in adsorption peaks at shorter wavelengths.[40] The effect of molecular weights can also be seen in the UV-vis data of Au@PS NP monolayers, as shown in Fig. S6† (λ_{max} of Au@$PS_{5.8k}$ monolayer = 543 nm, λ_{max} of Au@PS_{53k} monolayer = 537 nm).

Conclusions

In conclusion, we present a novel and facile method to fabricate hybrid Au@PS nanostructures with stable and controllable morphologies and optical properties. In the formation process, the Au@PS NPs acting as building blocks can be assembled into hybrid Au@PS nanotubes and hierarchical hybrid Au@PS nanospheres. Especially, the formation of the hierarchical hybrid Au@PS nanospheres is caused by both the nonsolvent-induced Rayleigh-instability-driven transformation and the confinement effect of the nanopores of the AAO templates. This strategy not only provides a feasible route to prepare hybrid polymer–Au nanostructures, but also allow us to access new ways of tailoring plasmonic coupling and magnetic dipolar coupling properties in three-dimensional nanoparticle assemblies. For the prepared hybrid nanostructures, we expect that they may have potential applications in areas such as sensing, drug delivery, and organic solar cells.[41,42]

Notes and references

1 R. Hao, R. J. Xing, Z. C. Xu, Y. L. Hou, S. Gao and S. H. Sun, *Adv. Mater.*, 2010, **22**, 2729–2742.
2 K. Saha, S. S. Agasti, C. Kim, X. N. Li and V. M. Rotello, *Chem. Rev.*, 2012, **112**, 2739–2779.
3 O. Veiseh, J. W. Gunn and M. Q. Zhang, *Adv. Drug Delivery Rev.*, 2010, **62**, 284–304.
4 S. Sarina, E. R. Waclawik and H. Y. Zhu, *Green Chem.*, 2013, **15**, 1814–1833.
5 J. T. Chen and C. S. Hsu, *Polym. Chem.*, 2011, **2**, 2707–2722.
6 F. Caruso, M. Spasova, V. Saigueirino-Maceira and L. M. Liz-Marzan, *Adv. Mater.*, 2001, **13**, 1090–1094.
7 M. Kim, K. Sohn, H. Bin Na and T. Hyeon, *Nano Lett.*, 2002, **2**, 1383–1387.
8 N. A. Lockwood, J. K. Gupta and N. L. Abbott, *Surf. Sci. Rep.*, 2008, **63**, 255–293.
9 X. L. Wang, Y. F. Bi, B. K. Chen, H. Y. Lin and G. C. Liu, *Inorg. Chem.*, 2008, **47**, 2442–2448.
10 R. Shenhar, T. B. Norsten and V. M. Rotello, *Adv. Mater.*, 2005, **17**, 657–669.
11 A. S. Urban, X. S. Shen, Y. M. Wang, N. Large, H. Wang, M. W. Knight, P. Nordlander, H. Y. Chen and N. J. Halas, *Nano Lett.*, 2013, **13**, 4399–4403.
12 P. X. Zhao, N. Li and D. Astruc, *Coord. Chem. Rev.*, 2013, **257**, 638–665.
13 J. C. Hulteen and C. R. Martin, *J. Mater. Chem.*, 1997, **7**, 1075–1087.
14 C. R. Martin, *Acc. Chem. Res.*, 1995, **28**, 61–68.
15 H. Masuda and K. Fukuda, *Science*, 1995, **268**, 1466–1468.
16 A. P. Li, F. Muller, A. Birner, K. Nielsch and U. Gosele, *J. Appl. Phys.*, 1998, **84**, 6023–6026.
17 A. C. Shi and B. H. Li, *Soft Matter*, 2013, **9**, 1398–1413.
18 K. Shin, H. Q. Xiang, S. I. Moon, T. Kim, T. J. McCarthy and T. P. Russell, *Science*, 2004, **306**, 76.
19 M. Steinhart, J. H. Wendorff, A. Greiner, R. B. Wehrspohn, K. Nielsch, J. Schilling, J. Choi and U. Gosele, *Science*, 2002, **296**, 1997.
20 V. M. Cepak and C. R. Martin, *Chem. Mater.*, 1999, **11**, 1363–1367.
21 S. L. Mei, X. D. Feng and Z. X. Jin, *Soft Matter*, 2013, **9**, 945–951.
22 J. T. Chen, C. W. Lee, M. H. Chi and I. C. Yao, *Macromol. Rapid Commun.*, 2013, **34**, 348–354.
23 C. W. Chang, M. H. Chi, C. W. Chu, H. W. Ko, Y. H. Tu, C. C. Tsai and J. T. Chen, *RSC Adv.*, 2015, **5**, 27443–27448.
24 J. T. Chen, K. Shin, J. M. Leiston-Belanger, M. F. Zhang and T. P. Russell, *Adv. Funct. Mater.*, 2006, **16**, 1476–1480.
25 X. D. Feng and Z. X. Jin, *Macromolecules*, 2009, **42**, 569–572.
26 M. Pasquali, J. Liang and S. Shivkumar, *Nanotechnology*, 2011, **22**, 10.
27 J. T. Chen, T. H. Wei, C. W. Chang, H. W. Ko, C. W. Chu, M. H. Chi and C. C. Tsai, *Macromolecules*, 2014, **47**, 5227–5235.
28 H. W. Ko, M. H. Chi, C. W. Chang, C. W. Chu, K. H. Luo and J. T. Chen, *ACS Macro Lett.*, 2015, **4**, 717–720.
29 M. C. Daniel and D. Astruc, *Chem. Rev.*, 2004, **104**, 293–346.
30 J. Turkevich, P. C. Stevenson and J. Hillier, *Discuss. Faraday Soc.*, 1951, **11**, 55–75.
31 G. Frens, *Nature*, 1973, **241**, 20–22.
32 Z. H. Nie, D. Fava, M. Rubinstein and E. Kumacheva, *J. Am. Chem. Soc.*, 2008, **130**, 3683–3689.
33 L. Weikun, L. Shanqin, D. Renhua and Z. Jintao, *Angew. Chem., Int. Ed.*, 2011, **50**, 5865–5868.
34 J. Plateau, *Translation in Annual Reports of the Smithsonian Institution*, 1873, 1863–1866.
35 L. Rayleigh, *Proc. Lond. Math. Soc.*, 1878, **10**, 4–13.
36 C. W. Lee, T. H. Wei, C. W. Chang and J. T. Chen, *Macromol. Rapid Commun.*, 2012, **33**, 1381–1387.
37 N. Yan, Y. P. Sheng, H. X. Liu, Y. T. Zhu and W. Jiang, *Langmuir*, 2015, **31**, 1660–1669.
38 S. R. Wasserman, H. Biebuyck and G. M. Whitesides, *J. Mater. Res.*, 1989, **4**, 886–891.
39 R. J. Liang, J. P. Xu, R. H. Deng, K. Wang, S. Q. Liu, J. Y. Li and J. T. Zhu, *ACS Macro Lett.*, 2014, **3**, 486–490.
40 H. Yockell-Lelievre, J. Desbiens and A. M. Ritcey, *Langmuir*, 2007, **23**, 2843–2850.
41 C. C. D. Wang, W. C. H. Choy, C. H. Duan, D. D. S. Fung, W. E. I. Sha, F. X. Xie, F. Huang and Y. Cao, *J. Mater. Chem.*, 2012, **22**, 1206–1211.
42 D. A. Giljohann, D. S. Seferos, W. L. Daniel, M. D. Massich, P. C. Patel and C. A. Mirkin, *Angew. Chem., Int. Ed.*, 2010, **49**, 3280–3294.